Optical anisotropy and magneto-optical properties of Ni on preoxidized Cu(110)

Th. Herrmann, K. Lüdge, and W. Richter
Institut für Festkörperphysik, Technische Universität Berlin, Hardenbergstraße 36, D-12049 Berlin, Germany

K. G. Georgarakis
Laboratory of Physical Metallurgy, National Technical University of Athens, Greece

P. Poulopoulos
Department of Materials Science, University of Patras, 26504 Patras, Greece

R. Nünthel and J. Lindner
Institut für Physik, Universität Duisburg-Essen, Lotharstrasse 1, D-47048 Duisburg, Germany

M. Wahl and N. Esser
ISAS-Institute for Analytical Sciences, Department Berlin, Albert-Einstein-Straße 9, D-12489 Berlin, Germany
(Received 19 September 2005; revised manuscript received 31 January 2006; published 7 April 2006)

We investigate the growth mode and the magnetism of Ni on Cu(110) substrates using oxygen as a surfactant. Layer by layer growth on oxidized Cu(110) is obtained, in contrast to the island growth found on clean Cu(110) substrates. The main emphasis of our work addresses the potential of optical spectroscopy for analyzing structure and magnetism. For that purpose we use a spectrometer which allows us to record reflectance anisotropy (RAS) and magneto-optic Kerr (MOKE) spectra simultaneously and *in situ* during film growth, in the spectral range from 0.72 to 6.5 eV. We show that RAS is very useful for monitoring the growth of Ni on Cu(110), since it reveals information on the atomic surface structure and on the strain evolution during the growth process. MOKE, on the other hand, is sensitive to the magnetic properties of the epitaxial Ni film. Combining RAS and MOKE thus allows us to directly relate growth mode and magnetic properties and to identify correlations in between. As such, an out-of-plane magnetization for Ni films between 7.5 and 35 ML thickness is observed, correlated with a flat layer morphology, i.e., two-dimensional growth mode of the Ni film. Above 35 ML roughening sets in and the magnetization direction rotates towards in-plane orientation again. Well below 35 ML, between 14 ML and 18 ML of Ni, the strain due to pseudomorphic growth is relaxed, correlated with a strong increase in coercivity due to dislocation formation. Mandatory for a meaningful analysis of the Voigt parameter of Ni is the sophisticated optical modeling of the layer system. Doing so, we prove that a modification of electronic properties (*d*-band narrowing) of the Ni film in the pseudomorphic growth regime does not occur, in contrast to expectations.

DOI: 10.1103/PhysRevB.73.134408 PACS number(s): 75.50.Cc, 78.20.−e, 78.66.Bz, 78.68.+m

I. INTRODUCTION

The growth of ferromagnetic thin films on nonmagnetic metallic substrates has attracted considerable attention in the last decade. A large number of studies focused on Ni films grown on Cu surfaces, mainly because of its interesting structural and magnetic properties. One of the most intensively studied systems in this field represents Ni on Cu(001), due to its favorable growth properties. In the following we briefly summarize the properties of Ni on Cu(001) before we turn to the less well understood case on Cu(110). It has been shown that the growth of Ni on Cu(001) is pseudomorphic at least up to eleven monolayers (ML), i.e., the lateral lattice parameter of the Ni film is enlarged with respect to that of a bulk crystal.[1–3] On such films, e.g., 20 Å (11 ML) Ni grown on Cu(001), a redshift in the off-diagonal conductivity spectra was observed. This was attributed to a narrowing of the 3*d* bands of Ni induced by the tetragonal distortion together with the reduced coordination number at the surface.[4]

The magnetic behavior of these films is abundantly reported in the literature. Up to 4 ML of Ni on Cu(001) no magnetization at room temperature (RT) was found,[5–8] since RT is higher than the Curie temperature of such thin Ni/Cu(001) films. Thicker Ni films up to 7 ML were found to be magnetic at RT with the easy axis of magnetization being located in the plane of the surface.[5,6,9] A spin reorientation transition from in plane to out of plane magnetization was found at a Ni thickness of 8–11 ML and interpreted as due to the thermodynamic interplay of different magnetic contributions such as surface, volume and shape anisotropy.[1,6,10–15] Above 15 ML of Ni a strong increase of the coercivity occurs attributed to the formation of dislocations.[16]

More recently, oxygen was shown to act as a surfactant and to modify the magnetic properties of Ni on Cu(001). A spin reorientation transition to out of plane at 4.9 ML, an onset of dislocation formation at 20 ML and another in plane reorientation transition for Ni films thicker than 40 ML, were reported.[6,16–19]

Comparably few studies have addressed Ni on Cu(110), in contrast to Cu(001). On Cu(110) Ni is known to grow in a

three-dimensional mode. Wu *et al.*[20] reported a critical thickness of 16 ML, below which the films have a dominant in-plane magnetization, while above it, the easy axis of magnetization turns out of plane. Sacchi *et al.*,[21] on the contrary, observed a fully remanent alignment of the Ni magnetic moment in the surface plane for the thickness range of 10–30 ML. Thus, in particular Ni on Cu(110), should be an interesting candidate for investigating the use of oxygen as a surfactant.

For our experiments we combine *in situ* studies by scanning tunneling microscopy (STM), low energy electron diffraction (LEED), and Auger electron spectroscopy (AES) with *in situ* optical spectroscopy. In particular we apply simultaneously reflectance anisotropy spectroscopy (RAS) and polar magneto-optic Kerr spectroscopy (MOKE).

Optical spectroscopy is a powerful tool, well suited for *in situ* analysis of surfaces and thin film growth. So far, RAS has been used primarily for studying semiconductors.[22,23] However, the potential of RAS for surface analysis of metals has been proven as well.[24–26] For (110) surfaces of fcc metals it was shown that electronic transitions between surface states and surface modified bulk states result in characteristic features to the optical anisotropy.[24,25] Furthermore, RAS is sensitive to symmetry reducing effects such as, e.g., atomic surface steps[27] and uniaxial stress within the surface plane.[28,29]

MOKE at a single photon wavelength, on the other hand, is a well established and powerful tool to investigate the magnetic properties of ferromagnetic layers.[3,12,20,30–34] MOKE spectroscopy can give useful information on the modification of the electronic structure,[4,35] but has rarely been used so far. Only recently, generalized ellipsometry was shown to be extremely useful for spectroscopic characterization of magneto-optical materials and layers.[36] Comparing with generalized ellipsometry, the combination of RAS and polar MOKE (one common setup operating under normal incidence) is the much simpler experimental method and better suited to analyze surface and ultrathin layer contributions. On the other hand, RAS/MOKE is less generally applicable, since it is limited to the optical anisotropy and to the polar Kerr effect. The full dielectric tensor cannot be determined with this approach, i.e., isotropic terms must be taken from other sources. Nevertheless, as we will demonstrate in the following, RAS and MOKE are an excellent combination for *in situ* analysis and control of ferromagnetic layer growth. One obtains real-time information during growth about electronic and magnetic properties.

II. EXPERIMENTAL DETAILS AND SAMPLE PREPARATION

The experiments were performed in an ultrahigh vacuum (UHV) system, equipped with STM, AES, RAS/MOKE, and LEED. For further details see Ref. 37. Clean Cu(110) substrates were prepared by approximately 25 repeated cycles of Ar^+ ion bombardment (1 keV, 10 min at room temperature) followed by subsequent annealing at 850 K. After that a well-ordered Cu(110)-(1×1) surface was obtained and no impurities could be detected with AES. The clean surface was exposed to 10 Langmuir of oxygen at room temperature to form the Cu(110)-(2×1)-O "added-row" structure.[38,39] Ni was evaporated at room temperature on the Cu(110)-(2×1)-O surface with a flux rate of 0.25 monolayers per minute. The thickness of the Ni layer was estimated with AES, by analyzing the relative heights of the Ni and Cu Auger intensities. For a fcc crystal the spacing of the (110) planes is $a_0\sqrt{2}/4$ (a_0: lattice constant), but in this work we define the layer thickness as $a_0\sqrt{2}/2$. This is reasonable for comparing the results with measurements on (001) oriented crystals.

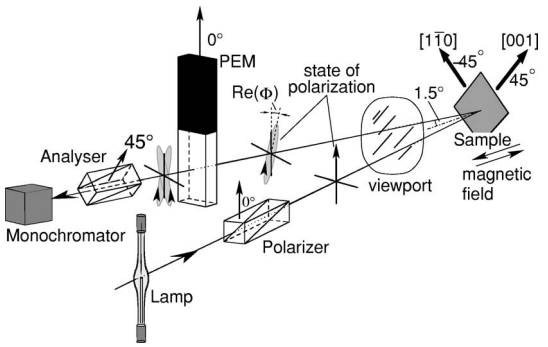

FIG. 1. Schematic diagram of the RAS/MOKE setup with a (110) oriented sample, as used in this work. The principal axis correspond to the [1$\bar{1}$0] and [001] directions. The angle of incidence is close to normal incidence (1.5°). The magnetic field is applied perpendicularly to the surface.

The optical measurements were done *in situ* through a low strain quartz view-port using one common spectrometer for RAS and polar MOKE spectroscopy. The birefringence contribution of the view-port was separated by calibration measurements on optically isotropic, paramagnetic samples, such as Cu(100). While this birefringence is very small (<2 mrad) for the RAS real part or the Kerr rotation, it is considerably larger for the imaginary part or the Kerr ellipticity. The discussion of experimental results will thus concentrate on the real parts of MOKE and RAS spectra. The spectrometer measures optical anisotropy and magneto-optical Kerr effect in an energy (wavelength) range from 0.75 to 6.5 eV (1653 nm to 190 nm). Hysteresis loops, RAS and MOKE transients (i.e., temporal evolution at a fixed wavelength) can be obtained at any desired energy within that spectral range. The optical setup itself (see Fig. 1) is analogous to other MOKE and RAS spectrometers.[40,41] New is in particular the handling and data processing for simultaneous recording of MOKE and RAS. The sample was illuminated near normal incidence (1.5°) with linearly polarized light. The state of polarization of the reflected light is analyzed by a combination of photoelastic modulator (PEM) and a fixed analyzer. The signal originates from the change of the polarization state, given by the polarization rotation Re(Φ) (real part of RAS and Kerr rotation), or the ellipticity Im(Φ) (imaginary part of RAS and Kerr ellipticity) of the reflected light. Apparatus settings determine whether polarization rotation or ellipticity are detected.[40,41]

III. MOKE-RAS MEASUREMENT SCHEME

RAS measures the difference of the complex reflectivity for linear polarization along two perpendicular axes $\vec{a}$ and $\vec{b}$ within the surface. The signal is defined as[40]

$$\frac{\Delta r}{r} = 2\frac{r_{\vec{a}} - r_{\vec{b}}}{r_{\vec{a}} + r_{\vec{b}}}. \tag{1}$$

In the geometry as shown in Fig. 1, $\vec{a}$ and $\vec{b}$ correspond to the $[1\bar{1}0]$ and $[001]$ directions within the surface plane of the sample. For small complex angles, $\Delta r/r$ is connected with the complex angle Φ_{RAS} by

$$\Phi_{\mathrm{RAS}} = \frac{\Delta r}{2r} \quad (\Phi_{\mathrm{RAS}} \ll 1). \tag{2}$$

For symmetry reasons, cubic crystals such as the fcc metals Ag, Cu, Ni, or hcp Co do not have a significant bulk contribution to the RAS signal. In such circumstances the RAS signal is mainly surface related.[22–26] In the case of a thin anisotropic surface layer (thickness $d \ll \lambda$) on an optically isotropic substrate, the RAS signal can be expressed by

$$\frac{\Delta r}{r} = \frac{-4\pi i d}{\lambda}\frac{\Delta\varepsilon}{\varepsilon_b - 1} \tag{3}$$

with the surface dielectric anisotropy (SDA) $\Delta\varepsilon \cdot d$ (Ref. 42) and the bulk dielectric function ε_b.

The Kerr effect originates from different optical "constants" for right- and left-circularly polarized light of a material in a magnetic field. Different complex reflectivities (r_+) and (r_-) are thus induced by a magnetization along the propagation direction of light. The magnetization related change in reflection of light is described with the complex Kerr angle Φ_{Kerr}.[43–45] Linear polarized light will be subjected to polarization change upon reflection since it refers to a superposition of two circularly polarized components. For normal incidence, as relevant here, only the out of plane component of the magnetization vector contributes to the MOKE signal (polar Kerr effect). Given a small difference in the complex reflectivity of right- and left-circularly polarized light, the polar Kerr effect is expressed by[46]

$$\Phi_{\mathrm{Kerr}} = i\frac{r_+ - r_-}{r_+ + r_-}. \tag{4}$$

For ultrathin ferromagnetic layers $[\mathrm{Re}(n_f)d \ll \lambda,\ n_f = \sqrt{\varepsilon_f}]$ the polar Kerr effect Φ_{Kerr} can be described by[45]

$$\Phi_{\mathrm{Kerr}} = \frac{4\pi Q d}{\lambda}\frac{\varepsilon_f}{\varepsilon_s - 1}, \tag{5}$$

where ε_f, ε_s are the dielectric functions of the film and the substrate, λ the wavelength of light, and Q the magneto-optic (Voigt) constant of the film. Equations (4) and (5) are derived for an optically isotropic film and substrate. In the present anisotropic case of a thin Ni film on a Cu substrate, one would have to calculate the Kerr effect for the two different dielectric functions $\varepsilon_{[1\bar{1}0]}$ and $\varepsilon_{[001]}$ separately. But since the optical anisotropy of the film and the surface are very small, below $10^{-3}\varepsilon$, the total change of polarization state $\Phi = \Phi_{\mathrm{Kerr}} + \Phi_{\mathrm{RAS}}$ is given by a linear superposition of optical anisotropy and Kerr effect to a very good approximation.

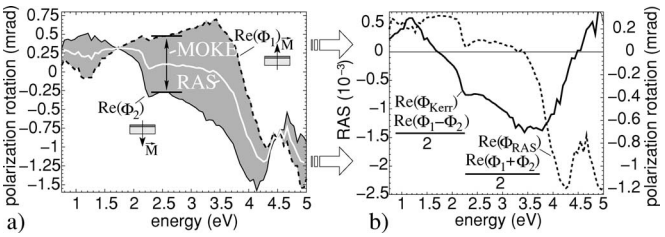

FIG. 2. (a) Polarization rotation spectrum recorded for 14 ML Ni on Cu(110)-O at two different magnetization directions $\vec{M}$. The direction of the magnetization for each spectrum is indicated in the figure. RAS and MOKE signals are shown as white line and as shaded area between the measurement curves, respectively. (b) MOKE and RAS spectra derived from the measured data (RAS signal of 0.001=0.5 mrad).

There are two possibilities to separate RAS and MOKE contributions from the measurement. RAS depends on the direction of the crystal axes towards the direction of the polarization of the incoming light. Thus a 90° rotation of the sample around the surface normal causes an inversion of the sign of Φ_{RAS}. MOKE on the contrary, depends only on the direction of the magnetization. Hence a turnaround of the out of plane magnetization changes the sign of the Kerr effect, while rotation around the surface normal does not have any effect. However, rotating of the sample often causes a misalignment of the optical setup. Therefore a turnaround of the magnetization is the preferred method to separate RAS and MOKE contributions. The measurement process is fully automated according to the following sequence: (1) applying (and switching off) a magnetic field to the sample perpendicular to the surface, (2) taking a first spectrum $[\mathrm{Re}(\Phi_1)]$, (3) applying (and switching off) a magnetic field in the reverse direction, and (4) taking a second spectrum $[\mathrm{Re}(\Phi_2)]$.

The RAS and MOKE signals are then given by

$$\mathrm{Re}(\Phi_{\mathrm{Kerr}}) = \mathrm{Re}(\Phi_1 - \Phi_2)/2 \text{ and } \mathrm{Re}(\Phi_{\mathrm{RAS}}) = \mathrm{Re}(\Phi_1 + \Phi_2)/2 \tag{6}$$

(see Fig. 2). Depending on the state of magnetization (on or off) during spectra acquisition either the nonremanent or remanent polar Kerr effect is detected.

At constant photon energies between 0.75 and 6.5 eV, MOKE and RAS transients can be recorded or, alternatively, MOKE hysteresis loops with a magnetic field up to 80 mT. For MOKE transients we used an external magnetic field of 40 mT.

IV. RESULTS

A. Surfactant effect of oxygen

STM measurements were performed to study the morphology and surface structure of freshly deposited Ni films on Cu(110) with and without oxygen preadsorption. Under UHV conditions, Ni was evaporated on the clean Cu(110)-(1×1) surface and on the Cu(110)-(2×1)-O sur-

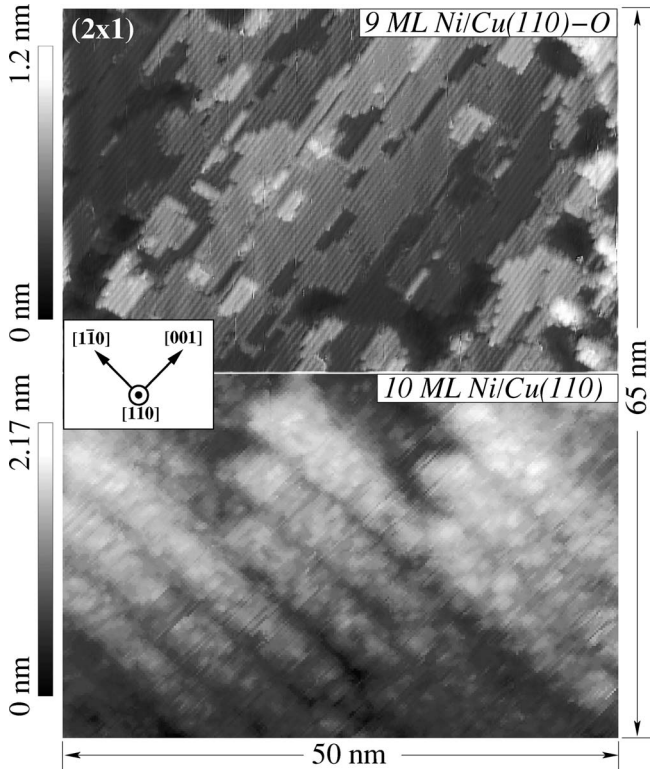

FIG. 3. STM images of Ni films grown on the preoxidized Cu(110)-(2×1)-O (top) and the clean Cu(110) surfaces. Surface directions and layer thickness are noted within the images. Bars at the left side denote the height scale. The LEED pattern (not shown here) of the Ni film on Cu(110)-(2×1)-O shows a (2×1) reconstruction with bright, sharp spots and low background.

face. Figure 3 shows two corresponding images obtained for Ni films of 9 and 10 ML thickness on preoxidized and clean Cu(110), respectively. A drastic influence of the oxygen on the Ni film morphology is immediately evident. Ni on clean Cu(110) grows in a very rough three-dimensional-(3D-)like mode in agreement with previous reports.[20,21,47] The Ni film forms long, one-dimensional-like structures extending along the [1$\bar{1}$0] direction (length: 20–50 nm, width: 4.5–6.5 nm). Within these structures we could not reach atomic resolution, because of the large roughness. On the contrary, 9 ML Ni on Cu(110)-(2×1)-O grows in a nearly ideal 2D fashion. STM reveals atomically flat terraces with long, straight atomic rows extending along the [001] direction. LEED images disclose a (2×1) reconstruction with bright, sharp spots on a low background. AES measurements show that the surface is approximately covered with half a monolayer of oxygen. STM, LEED, and AES results consistently suggest that oxygen acts as a surfactant, segregating to the surface of the Ni layer and inducing a layer-by-layer growth mode. A surfactant effect of oxygen has also been reported for Co/Cu(110) and Ni/Cu(001).[16,37] The surface structure of the oxygen terminated Ni(110) layer appears very similar to that of the Cu(110)-(2×1)-O surface (i.e., replacing Cu by Ni).

B. Optical anisotropy of Cu(110) and Ni(110)

The RAS spectra recorded on thin Ni films on Cu(110) consist of contributions of the surface, Ni film and the interface, assuming the layer thickness to be smaller than the penetration depth of light in nickel.

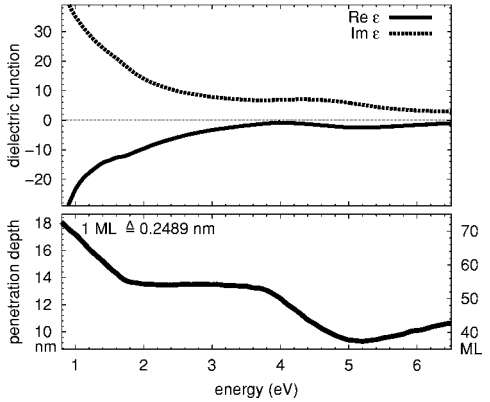

FIG. 4. Dielectric function (Ref. 48) (upper diagram) and the related penetration depth of light (lower diagram) of crystalline Ni.

Figure 4 shows the dielectric function of Ni and the penetration depth of light derived therefrom for the spectral range of 0.8 to 6.5 eV. For the following discussions it is worth noticing that the penetration depth varies between 10 and 18 nm, approximately corresponding to 40 and 70 ML of Ni. Consequently, when growing epitaxial Ni films on Cu(110), the optical anisotropy of the Ni-Cu interface will contribute to the RAS spectra up to several 10 ML of Ni thickness. In fact, this is observed as discussed in the next paragraph. Since the dielectric function (or optical "constant") of Ni is isotropic and does not show any pronounced structures in the spectral range studied here, the optical anisotropy of Ni(110) and Cu(110) surfaces and interfaces, respectively, should give the dominant contributions to the RAS spectra. Accordingly we firstly consider the optical anisotropy of the relevant surfaces. The optical anisotropy determined on the (110) surfaces of Ni and Cu single crystals with and without oxygen termination is shown in Fig. 5.

The spectral features of the RAS spectrum of Cu(110)-(2×1)-O have already been discussed in Ref. 37. Pronounced are the contribution of surface states and surface resonances at 1.9 and 2.75 eV and a strong structure near 6 eV which we presume is due to the Cu-O- bonding involving Cu 3*d* and O 2*p* orbitals.[49] Optical transitions from the Cu *d* bands occur in the energy range from 2.2 to 5 eV.

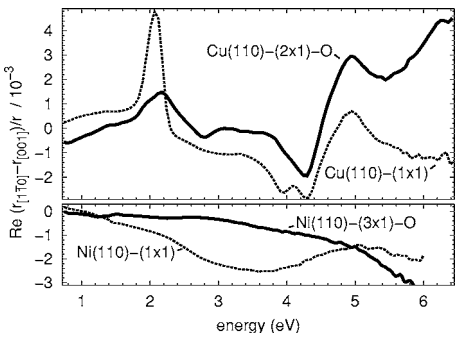

FIG. 5. RAS spectra of the clean and oxygen covered (110) surface of Cu and Ni. Cu(110) shows sharp spectral features, while Ni(110) exhibits only broad features.

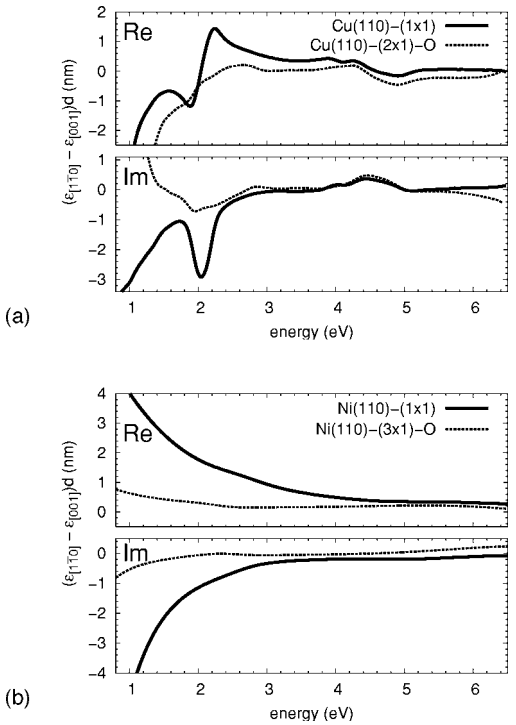

FIG. 6. Surface dielectric anisotropy (SDA) of Ni(110) and Cu(110) with and without oxygen coverage. Cu(110) exhibits sharp resonances in the measured spectral range, while Ni(110) is dominated by a Drude like contribution.

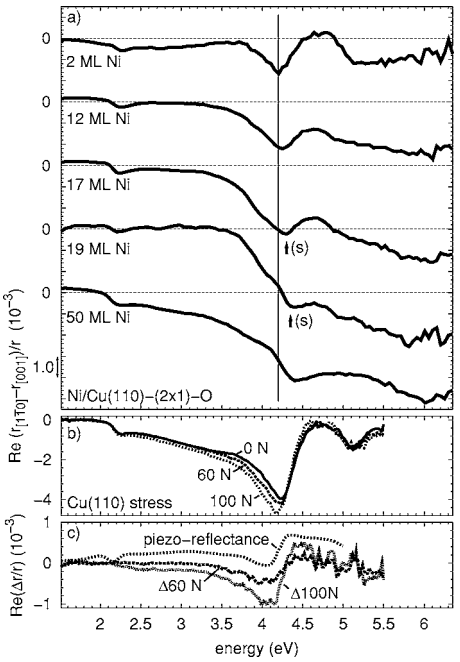

FIG. 7. RAS Spectra of Ni/Cu(110)-(2×1)-O in the thickness range from 2 to 50 ML Ni. Structure (*s*) is caused by strain within the copper substrate. (b) Optical anisotropy of Cu(110), obtained by stressing the crystal in [001] direction (ambient conditions). (c) Stress contribution to the optical anisotropy, derived from the difference of the spectra shown in (b), in comparison to the piezoreflectance measurements of amorphous copper.

These bulk states are anisotropically modified by the surface and contribute considerably to the optical anisotropy, because of their high density of states. A comparison of the RAS spectrum of Cu(110)-(2×1)-O shown here with the one published in Ref. 37 reveals some discrepancies below 1.3 eV. This is due to a not compensated offset of the infrared detector in the previous measurements.

The RAS spectra of Ni(110) depend on surface termination, but show only broad spectral features as compared to Cu(110). These differences are related to the specific electronic properties of Ni and Cu, as expressed by the surface and bulk electronic band structures. For Cu(110), the prominent structure around 2.1 eV in the optical anisotropy is mainly related to surface electronic transitions, while for Ni(110) there are no surface state transitions. The characteristic structures between 2.1 and 6 eV on Cu(110) are known to arise from electronic transitions of the filled *d*-band states, being located well below the Fermi energy, into empty conduction band states.[50] The *d* bands of Ni differ to the Cu case, since they overlap with the Fermi edge, being partly filled and exchange split.[51]

In order to separate surface and bulk influences to the lineshape of the RAS spectra we have calculated the surface dielectric anisotropy (SDA) (Fig. 6) according Eq. (3), using the optical constants of Ni and Cu published in Refs. 48, 50, and 52. In contrast to Cu(110), the SDA of Ni(110) is structureless apart from a pronounced Drude-like spectral dependence. This is quite interesting to note, since it shows that the free electrons of the metal are anisotropically modified by the surface. Here we would just like to emphasize that the optical anisotropy of Ni(110) has no distinct spectral features, in contrast to Cu(110).

The oxygen induced reconstruction on Ni(110) depends mostly on the O_2 dosage.[53] The (3×1) reconstruction shown here evolves after adsorption of more than four Langmuir oxygen. This reconstruction consists of double Ni-O rows in the [001] direction (two third of the surface is covered with O-Ni rows). We would like to note that the RAS spectrum of the oxygen covered (3×1) surface remains constant over several hours. In contrast, spectra of clean Ni surfaces change within minutes, due to dissociative adsorption of hydrogen. It was shown that the optical anisotropy of Ni(110)-(3×1)-O and Ni(110)-(2×1)-O is nearly identical.[54] This is the consequence of the fact that no surface state transitions are involved here, unlike the Cu(110)-O example.

C. Optical anisotropy of Ni layers on Cu(110)

Figure 7(a) shows the evolution of RAS spectra upon Ni deposition on the oxygen covered Cu(110) surface. After deposition of more than one monolayer of Ni, the surface state contribution of the Cu(110) surfaces is fully quenched. Thereafter, the remaining structures in the RAS spectra correspond to the Cu *d*-band transitions. Ni(110) does not show any distinct structures in the accessible spectral range, as discussed in the previous section. Dominating is the structure at 4.2 eV (denoted by "*s*"). As we will show in the following, this structure is indicative of the strain in the Cu(110)

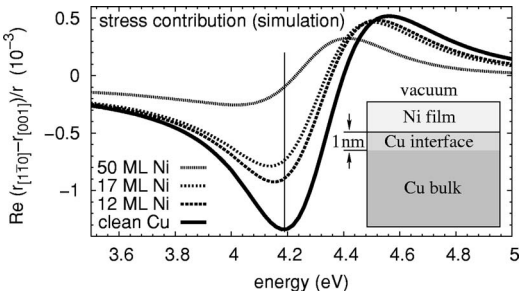

FIG. 8. Simulation of the RAS spectra of a vacuum/Ni-film/Cu(110)-interface/Cu(110) layer system with constant interface anisotropy (assumed to be related to strain) and increasing Ni capping layer thickness. The simulation algorithm is derived from that given by Azzam *et al.* (Ref. 57). Apparently the interface related structure shows a redshift with increasing layer thickness.

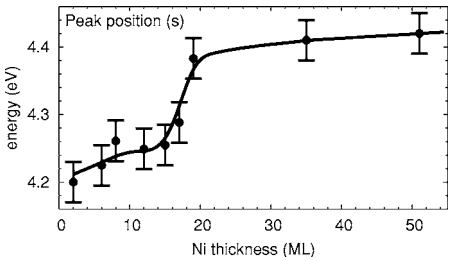

FIG. 9. Energetic position of the 4.3 eV RAS structure (*s*) as a function of Ni film thickness. The continuous line is just a guide to the eye. Vertical bar sizes denote error bars.

substrate. For comparison, Fig. 7(b) shows the strain contribution to the optical anisotropy of Cu(110) obtained by stressing the Cu(110) crystal in the [001] direction (under ambient conditions). As shown in Fig. 7(c), the strain related structure found using piezoreflectance on amorphous copper[55] is very similar to the one obtained in our RAS spectra after applying external stress. We would like to note that RAS measurements on the clean Cu(110) surface after different preparation cycles show such a strain contribution as well, indicating that Cu(110) is strained after preparation by sputtering and annealing. Thus we conclude that the structure (s) at 4.2 eV is caused by the strain within the copper substrate, which is partly induced by surface preparation and partly by an additional strain component due to the Ni layer in the pseudomorphic growth regime. The origin of the layer dependent strain at the Ni-Cu interface is the lattice mismatch of about 2.5% between the film and the substrate. Consequently, due to the anisotropic structure of the (110)-substrate plane one expects an uniaxial misfit strain within the surface plane, similar as reported for Co/Cu(110).[56]

As obvious in Fig. 7(a), the strain related structure shows a clear blueshift with increasing Ni layer thickness. Apart from the change of stress in the substrate, a spectral shift could alternatively be related to the change of the electromagnetic boundary conditions at the Ni/Cu interface through the replacement of vacuum by Ni. In order to address this effect, we have modeled the optical response of a four layer stack consisting of an isotropic Cu substrate, an anisotropic Cu interface region with a dielectric anisotropy derived from strained Cu(110), an isotropic capping layer of Ni with variable thickness, and vacuum surrounding. Figure 8 shows the simulated RAS spectra for a capping layer thickness up to 50 ML Ni. Optical constants of Ni and Cu are taken from Refs. 48, 50, and 52. The reflectivity is calculated for the [1$\bar{1}$0] and [001] directions separately, using an algorithm according to Azzam *et al.*[57] The resulting RAS signal is then defined by Eq. (1).

The simulation exhibits that, if the anisotropy at the interface remains constant, one should expect a damping and an energetic shift towards lower energies of the RAS structures with increasing Ni film thickness. This redshift is purely related to the multilayer structure, but not to a change in optical properties of one of the materials. Contrary to this scenario, the RAS spectra shown in Fig. 7 reveal a spectral shift of structure (*s*) towards higher photon energy with increasing Ni film thickness. We attribute the observed blueshift to a change of the strain at the Cu interface during Ni growth. Consequently, the spectral position of structure (*s*) is indicative of the change in interface strain during Ni growth. After the growth of several monolayers of Ni one expects a relaxation of the strained Ni film by evolving dislocations, as was found, e.g., on Ni/Cu(100).[6] The relaxation should lift the growth induced stress at the Ni/Cu interface.

Figure 9 displays the energy position of peak (s) as a function of Ni coverage. On the Ni/Cu(110)-O film peak (s) shifts strongly to higher energies between 16 and 18 ML and then saturates near 4.43 eV for higher film thickness. Thus we conclude that the strain of the Ni/Cu(110)-(2×1)-O film changes strongly, suggesting that the film relaxes between 16 and 18 ML of Ni.

The transient of the optical anisotropy at 2.1 eV during Ni growth shows a characteristic evolution with increasing Ni thickness (Fig. 10). We have repeated transient measurements several times and checked the thickness of the films with AES. From this we have confirmed that the RAS transients are extremely reproducible. The growth transient with-

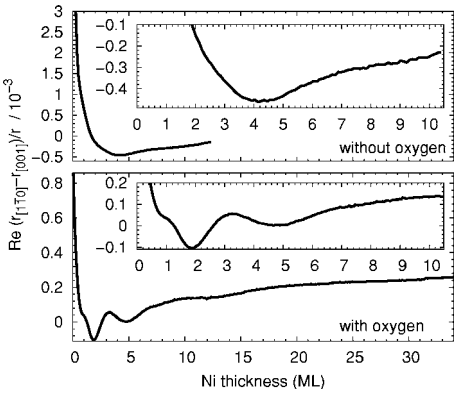

FIG. 10. RAS transient (online monitoring during Ni film growth) at 2.1 eV photon energy during Ni-film growth. The insets show the transients on an enlarged scale. Top: Growth on the Cu(110)-(1×1) surface. Bottom: Growth on the Cu(110)-(2×1)-O surface. Extrema in the RAS transient are most likely correlated with the formation of different epitaxial structures during the growth.

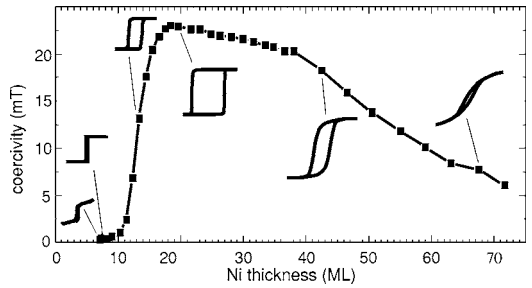

FIG. 11. Coercivity versus Ni film thickness and exemplary line shapes of the corresponding hysteresis loops taken at a photon energy of 3 eV. The coercivity increases strongly at coverages above 12 ML which suggests that the pseudomorphic growth ends at this thickness.

out oxygen shows a structureless decrease up to a minimum at 4 ML followed by a weaker, structureless increase above 4 ML. Up to 4 ML the transient reflects the quenching of the Cu(110) surface anisotropy, being indicative of a Ni island growth which appears to coalesce around 4 ML of Ni. In contrast thereto, the transient on the oxygen covered surface exhibits a strong decrease in the submonolayer coverage regime up to 0.9 ML, followed by several pronounced minima at 2 and 5 ML Ni and a weaker one around 15 ML.

From the Co/Cu(110)-(2×1)-O system we know that structural changes of the film reveal characteristic features in the RAS transient.[37] From that we conclude that different structural phases during the Ni growth are responsible for the characteristic RAS transient shape. On Co/Cu(110)-(2×1)-O it was found that Co first substitutes the Cu atoms in the Cu-O chains, followed by a reordering of the Co atoms and the formation of a Cu-O-Co interface structure.[58] A similar behavior most likely occurs for the Ni/Cu(110)-(2×1)-O growth. Further structures at 5 and 15 ML of Ni should be related to changes of the layer morphology. Around 5 ML a flattening of the Ni film occurs, while the minimum around 15 ML correlates with the relaxation of the Ni film. For a proof of this suggestion additional investigations, e.g., by STM, would be required.

To summarize the RAS results: The growth of Ni causes a quenching of the Cu(110) anisotropy. After 2 ML Ni a strain induced structure at 4.3 eV dominates the RAS spectra. This structure enables the monitoring of the strain within the substrate upon Ni growth. The results suggest that the film relaxes above a coverage of 15 ML of Ni. Moreover, the growth transients of Ni on Cu(110)-(2×1)-O exhibit characteristic structures correlated with the growth mode of the Ni layer.

D. Magnetic and magneto-optical properties

Figure 11 shows the coercivity change during Ni growth. This curve is derived from Kerr hysteresis loops obtained during short growth interruptions at a photon energy of 3 eV. To give an impression of the loop shapes, several loops are shown at selected Ni film thicknesses. For presentation purposes, the hysteresis loops are all scaled to the same size. Below 5.5 ML Ni we do not observe any Kerr signal. Between 5.5 and 7 ML Ni hard axis loops are obtained. Thus the film is ferromagnetic with the easy axis of the magnetization mainly parallel to the surface (in plane). The magnetization completely turns out of plane above 7.5 ML. Above 12 ML we observe a strong increase of the coercivity which saturates at 18 ML Ni. This behavior is similar to Ni on Cu(001).[6] Defects and dislocations induced by the film relaxation increase the coercive field.[6] From 18 to 35 ML the coercivity remains quite stable and hysteresis loops are perfectly rectangular, showing that the whole film is highly anisotropic with an easy axis perpendicular to the surface. Above 35 ML the coercivity decreases steadily and the loop shapes turn towards typical hard-axis hysteresis loops.

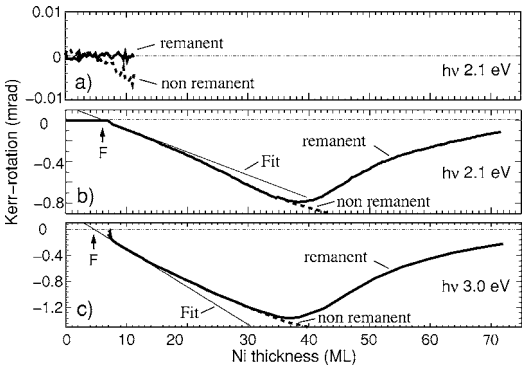

FIG. 12. Polar Kerr rotation without (remanent) and with (nonremanent) applied external magnetic field (40 mT) perpendicular to the surface plane, versus Ni film thickness. The transients were taken at a photon energy of 2.1 and 3 eV. An extrapolation of the Kerr intensity in the range from 8 to 12 ML (fit) defines the zero crossing point (F) (onset of ferromagnetism). (a) MOKE transient of the growth without oxygen and (b) MOKE transient of the growth with oxygen at a photon energy of 2.1 eV, (c) MOKE transient of the growth with oxygen at a photon energy of 3 eV, derived from hysteresis loops.

Figure 12 shows the polar Kerr rotation in remanence and with applied external magnetic field for the Ni growth with and without oxygen. Without oxygen, we cannot detect any remanent out of plane magnetization. The film is ferromagnetic above approximately 5 ML Ni with an in plane easy axis. In contrast thereto, Ni grown on the oxygen covered surface shows a remanent out of plane magnetization. An out of plane remanence firstly appears at 7 ML. Up to 7.5 ML the easy axis of the magnetization is only partly out of plane. This could be due to a tilted magnetization or due to the coexistence of different magnetic domains. For Ni coverages in the thickness range from 7.5 to 35 ML we observe a fully out-of-plane remanence.

Above 8 ML we observe a nearly linear increase of the remanence up to a Ni thickness of 35 ML. Since in the thin film limit ($d \ll \lambda$) the Kerr signal should be proportional to the thickness of ferromagnetic layers, the thickness of the nonmagnetic Ni layer (F) can be found from a linear extrapolation of the Kerr signal towards zero. Such linear fits are shown in Fig. 12 as straight thin lines, approximating the thickness range of 8 to 12 ML Ni. This analysis, however, fails and delivers inconsistent results, since the change in spectral line shape of the Kerr spectra with increasing Ni

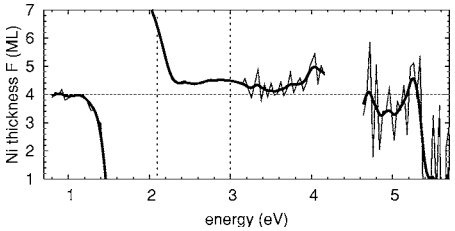

FIG. 13. Evaluation of the thickness (F) by linear extrapolation of the Kerr intensities of 8 and 12 ML Ni at different photon energies, derived from Kerr spectra (see Fig. 14). The thin lines show the not smoothed data, as derived from the measured spectra. Vertical lines denote the photon energies of the MOKE transients (see Fig. 12).

thickness, as discussed below in more detail, is neglected.

The dependence of the critical thickness derived from linear extrapolation and the spectral dependence of the MOKE signal becomes most evident in Fig. 13. Here the onset thickness of ferromagnetism was evaluated from polar Kerr spectra of 8 and 12 ML Ni as a function of photon energy in the fully accessible spectral range from 0.7 to 6.5 eV. The linear extrapolation of the onset thickness (F) fails in particular in the spectral region between 1.2 and 2.2 eV. Below 1.2 and above 2.2 eV, to the contrary, the extrapolation yields a consistent onset thickness of ferromagnetism of 4 ML Ni.

The spectral analysis of the Kerr effect (Fig. 14) allows us to resolve that puzzle. The polar magneto-optic Kerr spectra were recorded at magnetic remanence for 8–71 ML Ni films on Cu(110)-O(2×1). The spectral structures, in particular the zero crossing of the Kerr spectra between 1.2 and 2.2 eV, exhibit a redshift with increasing film thickness. We would like to note that this finding corroborates with the observation of Nakashima *et al.* reported for thin pseudomorphic Ni films on Cu(100) substrates.[4] As a consequence, the linear extrapolation of Kerr rotation as a function of film thickness [thin film limit, see Eq. (5)] is invalid in the spectral range where the line shape depends on thickness. The approximation is sufficiently fulfilled only in parts of the spectral range, particularly below 1.2 and above 2.2 eV.

The observed changes in the line shape of Kerr spectra referring to the optical properties of the layer system may be

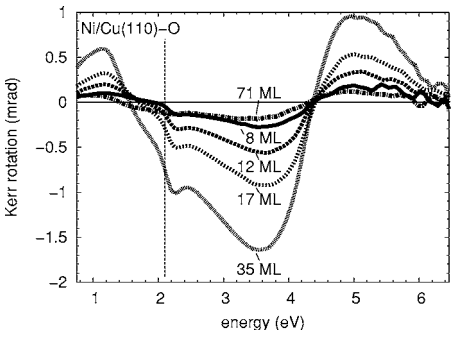

FIG. 14. Polar MOKE spectra (rotation) of 8–71 ML Ni on Cu(110)-O(2×1). The vertical line at 2.1 eV marks the energy at which the MOKE transient from Figs. 12(a) and 12(b), is recorded. All spectra are recorded at remanence. The low Kerr amplitude at 71 ML Ni is due to the in-plane reorientation of magnetization.

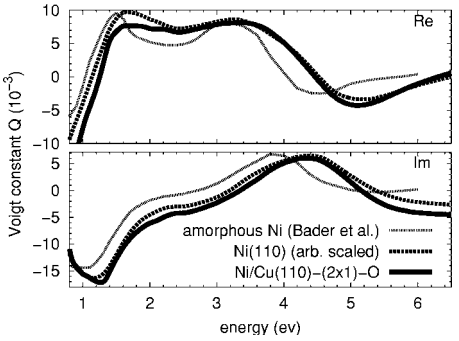

FIG. 15. Spectral dependence of Voigt constant for nominally 35 ML Ni (this work), single crystalline Ni (this work) and an amorphous Ni film [Bader *et al.* (Ref. 45)].

related to the increase in thickness as well as to possible changes of magneto-optical properties of the Ni layer. In order to separate both effects of thickness and magneto-optical properties one has to calculate the Voigt "constants" (which is a material specific, spectrally varying function) of the Ni film. This can be done in a four-layer optical model (vacuum/Ni_{ferro}/$Ni_{nonferro}$/Cu) (Ref. 44) using the experimentally determined real and imaginary parts of the Kerr coefficient Φ_{Kerr} and the dielectric function of Ni and Cu.[48,50] Figure 15 shows the resulting real and imaginary parts of a 35-ML-thick film in comparison with the Voigt constants of a Ni single crystal and of an amorphous layer.[45] As clearly evident, the Voigt constants of the epitaxial film correspond remarkably well to those of crystalline Ni, whereas amorphous Ni shows a substantially different spectral dependence. This result should be expected as the film of 35 ML nominal coverage corresponds to a relaxed crystalline Ni film, i.e., the lattice parameter is close to the bulk one. By using the such determined Voigt constants of crystalline Ni we have then modeled the Kerr rotation for various Ni thickness in order to compare with the experimentally determined curves. An according stack of data sets and modeled spectra is shown in Fig. 16. Apart from a slight deviation of the Ni film thickness between experiment and modeling the simulated Kerr rotation spectra show a remarkably good agreement with the experimental curves. The systematic deviation in Ni thickness simply points towards a small error in the thickness calibration of the Ni evaporator. The excellent agreement between simulated and experimental spectra, for thin pseudomorphic as well as for thick relaxed films, is quite an interesting result. This in fact means that the former interpretation of strain-related d-band narrowing in the Ni layer inducing changes in the Kerr spectra[4] is incorrect. The change in magneto-optical constants related to strain is not detectable, and the thickness dependence in Kerr rotation is just associated with an optical multilayer effect of the layer stack.

Summarizing, the magnetic properties of Ni on Cu(110)-O(2×1) differ in dependence of film thickness. (1) $\leqslant$4 ML: most likely, nonferromagnetic (or above Curie temperature), (2) $>$4 ML$\leqslant$7 ML: ferromagnetic, easy axis in plane, (3) $>$7 ML$\leqslant$7.5 ML: ferromagnetic, easy axis partly out of plane, (4) $>$7.5 ML$\leqslant$10 ML: ferromagnetic, easy axis out of plane, weak coercivity,

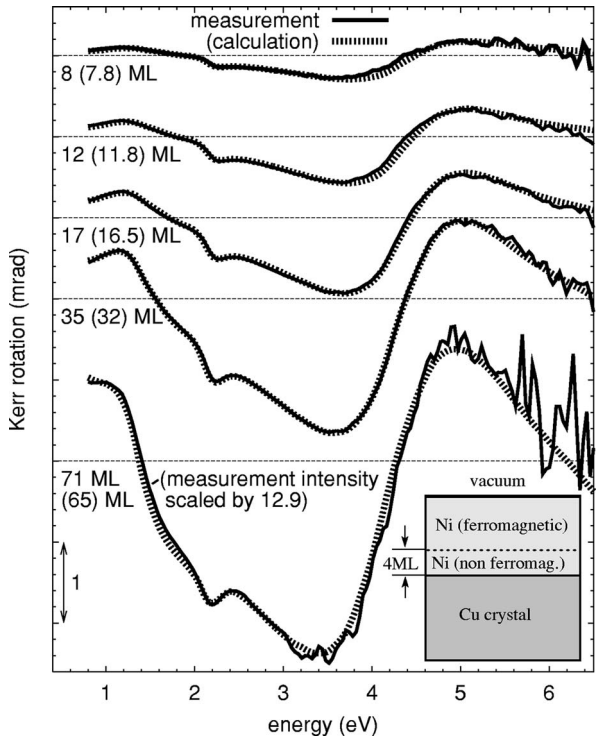

FIG. 16. Simulated polar MOKE spectra (rotation) for various Ni thickness in comparison with experimental ones. The Ni thickness in the optical modeling was taken as a free parameter to optimize modeling. The data set for Voigt constants and dielectric functions is the same for all modeled Kerr spectra. A four-layer system (vacuum/Ni_{ferro}/$Ni_{nonferro}$/Cu), according the diagram shown on the bottom right, was used for the simulation. Please note that the amplitude for the 71 ML spectrum is upscaled by 12.9.

(5) $>$10 ML$\leqslant$18 ML: strong increase of the coercivity, (6)$>$18 ML$\leqslant$35 ML: saturation of the coercivity, highly anisotropic Ni film, (7) $>$35 ML: partly in plane magnetization.

Remanent out of plane magnetization is only obtained when the surface termination by oxygen is present during the layer growth, while subsequent oxygen exposure on Ni films grown on clean Cu(110) does not influence the magnetization. This means that the related morphology changes rather than the presence of surface oxygen induces out-of-plane magnetization. For Ni films grown with a partial surface termination of 0.5–5% oxygen (not shown here) we find a partly out of plane orientation of the easy axis. Thus we conclude that the layer-by-layer growth mode of the Ni film is the essential prerequisite for the reorientation to out of plane magnetization. Partly out-of-plane magnetization could most likely be related to a laterally inhomogeneous growth mode for a too low surfactant concentration. We suggest that the contradictory results in Refs. 20 and 21 about the orientation of the easy axis of magnetization for Ni/Cu(110) (see Introduction) may most likely related to the presence of a small surface contamination (e.g., oxygen).

V. SUMMARY

We have successfully combined RAS/MOKE spectroscopy and STM to investigate the growth and magnetic properties of Ni/Cu(110)-O(2×1) films. It was shown that oxygen acts as a surfactant on Ni/Cu(110). From MOKE spectra and transients we find that the layer becomes ferromagnetic after the fourth monolayer of Ni. An out of plane orientation of the magnetization occurs in a thickness range from 7.5 to 35 ML of Ni. The pseudomorphic layer-by-layer-growth rather than the presence of oxygen at the surface is important for the occurrence of remanent out of plane magnetization on Ni/Cu(110).

We find features in RAS spectra that are clearly related with growth-induced strain in the Cu substrate. The analysis of these strain dependent structures together with the coercivity of the Ni overlayer shows that the film relaxes at Ni coverages around 12 to 18 ML. Moreover we show that the magneto-optical constants of the Ni films are not distinct from Ni bulk crystals. In particular no significant dependence on layer thickness or on tetragonal distortion related with pseudomorphic growth is found.

ACKNOWLEDGMENTS

This work was supported by the SFB 290 of the Deutsche Forschungsgemeinschaft (DFG), the Bundesministerium für Bildung und Forschung and the Senatsverwaltung für Wissenschaft, Forschung und Kultur des Landes Berlin. K.G. Georgarakis gratefully acknowledges Dr. Dimitra Papadimitriou for her support. He also wishes to thank the program "HAS" and the EU program "ERASMUS" for financial support. We would like to thank Dr. Kurt Hingerl for many valuable discussions concerning strain effects on RAS.

[1] W. Platow, U. Bovensiepen, P. Poulopoulos, M. Farle, M. F. K. Baberschke, L. Hammer, S. Walter, S. Müller, and K. Heinz, Phys. Rev. B **59**, 12641 (1999).
[2] S. Müller, B. Schulz, G. Kostka, M. Farle, K. Heinz, and K. Baberschke, Surf. Sci. **364**, 235 (1996).
[3] F. Huang, M. T. Kief, G. J. Mankey, and R. F. Willis, Phys. Rev. B **49**, 3962 (1994).
[4] K. Nakajima, H. Sawada, T. Katayama, and T. Miyazaki, Phys. Rev. B **54**, 15950 (1996).
[5] W. L. O'Brien and B. P. Tonner, Phys. Rev. B **49**, 15370 (1994).
[6] W. L. O'Brien, T. Droubay, and B. P. Tonner, Phys. Rev. B **54**, 9297 (1996).
[7] L. Tjeng, Y. Idzerda, P. Roudolf, F. Sette, and C. Chen, J. Magn. Magn. Mater. **54**, 288 (1992).
[8] P. Srivastava, F. Wilhelm, A. Ney, M. Farle, H. Wende, N. Haack, G. Ceballos, and K. Baberschke, Phys. Rev. B **58**, 5701 (1998).
[9] B. Schulz and K. Baberschke, Phys. Rev. B **50**, 13 467 (1994).
[10] S. van Dijken, R. Vollmer, B. Poelsema, and J. Kirschner, J. Magn. Magn. Mater. **210**, 316 (2000).
[11] O. Hjortstam, K. Baberschke, J. M. Wills, B. Johansson, and O.

Eriksson, Phys. Rev. B **55**, 15 026 (1997).
[12] S. Wu, G. Mankey, F. Huang, and R. Willis, J. Appl. Phys. **76**, 6434 (1994).
[13] R. Naik, C. Kota, J. S. Payson, and G. L. Dunifer, Phys. Rev. B **48**, 1008 (1993).
[14] M. Farle, W. Platow, A. N. Anisimov, P. Poulopoulos, and K. Baberschke, Phys. Rev. B **56**, 5100 (1997).
[15] K. Baberschke and M. Farle, J. Appl. Phys. **81**, 5038 (1997).
[16] R. Nünthel *et al.*, Surf. Sci. **531**, 53 (2003).
[17] J. Lindner, P. Poulopoulos, R. Nünthel, E. Kosubek, H. Wende, and K. Baberschke, Surf. Sci. Lett. **523**, L65 (2003).
[18] J. Lindner, P. Poulopoulos, M. Farle, and K. Baberschke, J. Magn. Magn. Mater. **218**, 10 (2000).
[19] P. Poulopoulos, M. Farle, U. Bovensiepen, and K. Baberschke, Phys. Rev. B **55**, R11961 (1997).
[20] S. Wu, G. Mankey, and R. Willis, J. Vac. Sci. Technol. A **13**, 1497 (1995).
[21] M. Sacchi, A. Minore, and S. Iacobbucci, Surf. Sci. **442**, 349 (1999).
[22] A. I. Shkrebtii, N. Esser, W. Richter, W. G. Schmidt, A. Kley, F. Bechstedt, B. Fimland, and R. Del Sole, Phys. Rev. Lett. **81**, 721 (1998).
[23] W. Richter and J.-T. Zettler, Appl. Surf. Sci. **100**, 465 (1996).
[24] K. Stahrenberg, T. Herrmann, N. Esser, and W. Richter, Phys. Rev. B **61**, 3043 (2000).
[25] P. Hofmann, K. C. Rose, V. Fernandez, A. M. Bradshaw, and W. Richter, Phys. Rev. Lett. **75**, 2039 (1995).
[26] J.-K. Hansen, J. Bremer, and O. Hunderi, Surf. Sci. **418**, L58 (1998).
[27] F. Baumberger, T. Herrmann, A. Kara, S. Stolbov, N. Esser, T. Rahman, J. Osterwalder, W. Richter, and T. Greber, Phys. Rev. Lett. **90**, 177402 (2003).
[28] R. Cole, S. Kheradmand, D. Higgins, F. Madani, B. Macdonald, V. Koutsos, and J. Blackford, J. Phys. D **36**, L115 (2003).
[29] L. Lastras-Mart1nez, R. Balderas-Navarro1, A. Lastras-Mart1nez, and K. Hingerl, Semicond. Sci. Technol. **19**, R35 (2004).
[30] M. Farle, A. Berghaus, Y. Li, and K. Baberschke, J. Magn. Magn. Mater. **93**, 215 (1991).
[31] Z. Qui and S. Bader, J. Magn. Magn. Mater. **200**, 664 (1999).
[32] P. Poulopoulos, M. Farle, U. Bovensiepen, and K. Baberschke, J. Magn. Magn. Mater. **177-181**, 1225 (1998).
[33] X. Liu, A. Berger, and M. Wuttig, Phys. Rev. B **63**, 144407 (2001).
[34] J. Zak, E. Moog, C. Liu, and S. Bader, J. Magn. Magn. Mater. **89**, 107 (1990).
[35] Š. Višňovský, M. Nývlt, V. Prosser, R. Lopušník, R. Urban, J. Ferré, G. Pénissard, D. Renard, and R. Krishnan, Phys. Rev. B **52**, 1090 (1995).
[36] G. Neuber, R. Rauer, J. Kunze, T. Korn, C. Pels, G. Meier, U. Merkt, J. Bäckstrom, and M. Rübhausen, Appl. Phys. Lett. **83**, 4509 (2003).
[37] T. Herrmann, K. Lüdge, W. Richter, N. Esser, P. Poulopoulos, J. Lindner, and K. Baberschke, Phys. Rev. B **64**, 184424 (2001).
[38] D. J. Coulman, J. Wintterlin, R. J. Behm, and G. Ertl, Phys. Rev. Lett. **64**, 1761 (1990).
[39] K. Kern, H. Niehus, A. Schatz, P. Zeppenfeld, J. Goerge, and G. Comsa, Phys. Rev. Lett. **67**, 855 (1991).
[40] D. E. Aspnes, J. P. Harbison, A. A. Studna, and L. T. Florez, J. Vac. Sci. Technol. A **6**, 1327 (1988).
[41] K. Sato, Jpn. J. Appl. Phys. **20**, 2403 (1981).
[42] K. Hingerl, D. E. Aspnes, I. Kamiya, and L. T. Florez, Appl. Phys. Lett. **63**, 885 (1993).
[43] E. R. Moog, J. Zak, M. L. Huberman, and S. D. Bader, Phys. Rev. B **39**, 9496 (1989).
[44] J. Zak, E. G. Moog, C. Liu, and S. D. Bader, Phys. Rev. B **43**, 6423 (1991).
[45] S. D. Bader, J. Magn. Magn. Mater. **100**, 440 (1991).
[46] A. Vernes, L. Szunyogh, and P. Weinberger, Phys. Rev. B **65**, 144448 (2002).
[47] R. Nünthel, J. Lindner, P. Poulopoulos, and K. Baberschke, Surf. Sci. **566-568**, 100 (2004).
[48] E. D. Palik, *Handbook of Optical Constants of Solids II* (Academic, San Diego, CA, 1991).
[49] R. Courths, S. Hüfner, P. Kemkes, and G. Wiesen, Surf. Sci. **376**, 43 (1997).
[50] K. Stahrenberg, T. Herrmann, K. Wilmers, N. Esser, W. Richter, and M. J. G. Lee, Phys. Rev. B **64**, 115111 (2001).
[51] D. E. Eastman, F. J. Himpsel, and J. A. Knapp, Phys. Rev. Lett. **40**, 1514 (1978).
[52] K. Stahrenberg, Ph.D. thesis, Technische Universität Berlin, Germany, 2000.
[53] H. Bu, C. Roux, and J. Rabalais, J. Chem. Phys. **97**, 1465 (1992).
[54] J.-K. Hansen, Ph.D. thesis, Norges teknisk-naturvitenskapelige universitet, Trondheim, Norway, 2000.
[55] M. Garfinkel, J. Tiemann, and W. Engeler, Phys. Rev. **148**, 695 (1966).
[56] J. Fassbender, G. Guntherodt, C. Mathieu, B. Hillebrands, R. Jungblut, J. Kohlhepp, M. T. Johnson, D. J. Roberts, and G. A. Gehring, Phys. Rev. B **57**, 5870 (1998).
[57] R. M. A. Azzam and N. B. Bashara, *Ellipsometry and Polarized Light, Paperback Edition* (North-Holland Personal Library, Amsterdam, 1987).
[58] W. L. Ling, O. Takeuchi, D. Ogletree, Z. Qiu, and M. Salmeron, Surf. Sci. **450**, 227 (2000).